Photocycle and Photoreversal of Photoactive Yellow Protein at Alkaline pH: Kinetics, Intermediates, and Equilibria†

Chandra P. Joshi,‡ Berthold Borucki,‡ Harald Otto,‡ Terry E. Meyer,§ Michael A. Cusanovich,§ and Maarten P. Heyn*,‡

Biophysics Group, Department of Physics, Freie Universität Berlin, Arnimallee 14, 14195 Berlin, Germany, and Department of Biochemistry and Molecular Biophysics, University of Arizona, Tucson, Arizona 85721

Received August 28, 2005; Revised Manuscript Received February 10, 2006

ABSTRACT: Since the habitat of *Halorhodospira halophila* is distinctly alkaline, we investigated the kinetics and intermediates of the photocycle and photoreversal of the photoreceptor photoactive yellow protein (PYP) from pH 8 to 11. SVD analysis of the transient absorption time traces in a broad wavelength range (330−510 nm) shows the presence of three spectrally distinct species (I_1, I_1', and I_2') at pH 10. The spectrum of I_1' was obtained in two different ways. The maximal absorption is at 425 nm. I_1' probably has a deprotonated chromophore and may be regarded as the alkaline form of I_2'. At pH 10, the I_1 intermediate decays in ∼330 μs in part to I_1' before I_1 and I_1' decay further to I_2' in ∼1 ms. From the rise of I_2' (∼1 ms) to the end of the photocycle, the three intermediates (I_1, I_1', and I_2') remain in equilibrium and decay together to P in ∼830 ms. Assuming that the spectra of I_1, I_1', and I_2' are pH-independent, their time courses were determined. On the millisecond to second time scale, they are in a pH-dependent equilibrium with a pK_a of ∼9.9. With an increase in pH, the I_1 and I_1' populations increase at the expense of the amount of I_2'. The apparent rate constant for the recovery of P slows with an increase in pH with a pK_a of ∼9.7. The equal pH dependence of this rate and the equilibrium concentrations follows, if we assume that the equilibration rates between the intermediates are much faster than the recovery rate and that the recovery occurs from I_2'. The pK_a of ∼9.9 is assigned to the deprotonation of the phenol of the surface-exposed chromophore in the $I_1'-I_2'$ equilibrium. The I_1-I_1' equilibrium is pH-independent. Photoreversal experiments at pH 10 with the second flash at 355 nm indicate the presence of only one I_2-like intermediate, which we assign on the basis of its λ_{max} value to I_2'. After the rapid unresolved photoisomerization to $I_2'^{trans}$, the reversal pathway back to P involves two sequential steps (60 μs and 3 ms). The amplitude spectra show that $I_1'^{trans}$ and I_1^{trans} intermediates participate in this reversal.

The blue light receptor photoactive yellow protein (PYP)[1] is an attractive model system for signal transduction (*1*, *2*). It is a small water soluble protein (125 residues, 14 kDa) that has *trans*-*p*-hydroxycinnamic acid covalently bound via a thioester linkage to cysteine 69 as its chromophore. Its structure, as determined by X-ray diffraction (*3*−*6*) and NMR (*7*), has a mixed α/β fold with a central six-stranded antiparallel β-sheet. PYP is now recognized as the structural prototype for a large and diverse family of sensory and signaling proteins that contain the PAS sequence motif (*8*). In the dark, the phenol group of the chromophore is deprotonated and the C_7═C_8 bond is trans. The phenolate oxygen is hydrogen-bonded to tyrosine 42 and the protonated carboxy group of glutamate 46. The deprotonation of the chromophore makes a major contribution to the spectral tuning in the dark state (λ_{max} ∼ 446 nm). Light-induced trans−cis isomerization around the C_7═C_8 bond is rapid (<3 ps) and is followed by a sequence of thermal relaxations ultimately leading back to the initial dark state. This photocycle has been studied in considerable detail (*9*−*11*). The first long-lived intermediate, after the two very short-lived intermediates (I_0 and $I_0^{‡}$), is I_1, which forms in ∼3 ns and has a red-shifted absorption spectrum (λ_{max} ∼ 460 nm). In several hundred microseconds, it decays to I_2, which has a protonated chromophore and a blue-shifted absorption spectrum (λ_{max} ∼ 370 nm) (*12*; B. Borucki et al., manuscript to be published). In I_2, the chromophore phenol is partially exposed to the aqueous medium and hydrogen-bonded to the side chain of R52 (*6*). The protonation of the chromophore occurs either intramolecularly from E46 (*13*) or from the external medium (*14*). In several milliseconds, I_2 is transformed into I_2' that is believed to be the signaling state. It also has a protonated chromophore with a λ_{max} value that is further blue shifted to ∼350 nm (*12*; B. Borucki et al., manuscript to be published). The I_2 to I_2' transition is associated with a major global structural change which has been documented by NMR (*15*), CD (*16*), small-angle X-ray scattering (*17*), and FTIR (*13*, *18*). Formation of I_2' is associated with exposure of a hydrophobic surface patch (*19*),

† This work was supported by NIH Grant GM 66146 (to M.A.C.) and DFG Grants HE 1382/13-1 and GK 788 TP A9 (to M.P.H.).

* To whom correspondence should be addressed. E-mail: heyn@physik.fu-berlin.de. Phone: +49-30-83856160. Fax: +49-30-83856299.

‡ Freie Universität Berlin.

§ University of Arizona.

[1] Abbreviations: SVD, singular-value decomposition; PYP, photoactive yellow protein; PAS domain, acronym formed from the names of the first three proteins recognized as sharing this sensory domain.

10.1021/bi0517335 CCC: $33.50
Published on Web 05/17/2006

presumably the recognition and binding site for a response regulator. Experiments with hydrophobic dyes showed that these bind transiently to I_2' but not to I_2 (*14*).

For an understanding of the mechanism of PYP, a detailed characterization of its photocycle is essential. Such studies have been carried out by both electronic (*9*−*11*, *20*) and vibrational (*13*, *18*, *21*, *22*) spectroscopy. The photocycle kinetics is pH-dependent (*23*, *24*) and salt-dependent (*25*, *26*). Whereas early models assumed a unidirectional sequential mechanism (*9*, *20*), it is becoming increasingly clear that back reactions and equilibria between intermediates play a significant role (*11*, *24*, *27*). These equilibria are also pH-dependent (*24*, *25*, *27*) and salt-dependent (*25*). The functionally important equilibrium between I_2 and I_2', the formation of the signaling state, is both salt-dependent (*25*) and pH-dependent with a pK_a of 6.2 (*12*; B. Borucki et al., manuscript to be published). Most photocycle intermediates can be photoreversed when excited with light of the appropriate wavelength at the right time (*28*, *30*).

The rate constant for the ground-state recovery has a bell-shaped pH dependence with apparent pK_a values of 6.4 and 9.4 (*23*). The nature of the group(s) responsible for these pK_a values is not entirely certain, but they have been assigned to E46 and the chromophore, respectively (*37*, *38*). Here we study the photocycle kinetics and intermediate equilibria in the alkaline pH range from pH 8 to 11 with transient absorption spectroscopy. Using SVD methods and other recently developed data analysis methods (*31*), we determined the intermediate spectra and the time dependence of the intermediate concentrations. In addition, we investigated the kinetics of photoreversal. Since the habitat of *Halorhodospira halophila* is distinctly alkaline, it is important to know the kinetics and intermediates in the alkaline pH range. Another functionally significant question concerns the pK_a above which the signaling state I_2' no longer accumulates. This determines the working pH range for signal transduction. Finally, it is important to understand the underlying cause for the pK_a of the ground-state recovery rate. By measuring the photocycle kinetics from 330 to 510 nm, we find that the I_2 intermediate is absent at alkaline pH but that an intermediate I_1' is formed from I_1 in 330 μs at pH 10, which absorbs maximally at 425 nm. On the millisecond time scale, all three intermediates (I_1, I_1', and I_2') are in equilibrium and decay together to the ground state P. With an increase in pH, the I_2' and I_1' populations in this equilibrium decrease and increase, respectively, with a pK_a of ~9.9. We find that the pK_a for the rate constant of recovery of P is a consequence of the pH dependence of the I_1'−I_2' equilibrium. This common pK_a is assigned to the partially exposed chromophore phenol group.

MATERIALS AND METHODS

Protein Production and Purification. H. halophila holo-PYP was produced by coexpression with the biosynthetic enzymes TAL and pCL and subsequently purified from *Escherichia coli* BL21(DE3) as described previously (*32*).

Transient Absorption Spectroscopy. Time-resolved absorption spectroscopy with single- and double-flash excitation was performed as described previously (*14*, *24*, *30*, *33*). To resolve the photoreversal kinetics, the data acquisition was triggered on the second flash. SVD methods were used as described previously (*14*, *24*, *34*−*36*).

Data Analysis. Spectra and time courses of intermediates were obtained as described previously (*31*). Since these procedures play an essential role in this work, they need to be briefly summarized. The transient absorbance change $\Delta A(\lambda,t)$ is given by

$$\Delta A(\lambda,t) = \sum_i [A_i(\lambda) - A_p(\lambda)] n_i(t) \quad (1)$$

where $A_i(\lambda)$, is the spectrum of intermediate i, $A_p(\lambda)$ is the spectrum of the dark state P, and $n_i(t)$ is the relative concentration of intermediate i. For photocycle schemes with first-order kinetics, the relative intermediate concentrations can be represented by a sum of exponentials:

$$n_i(t) = \sum_{j=1}^{r} C_{ij} e^{-t/\tau_j} \quad (2)$$

where r is the number of exponential components j necessary to fit the time traces. Substituting eq 2 in eq 1, we can rewrite eq 1 as

$$\Delta A(\lambda,t) = \sum_{j=1}^{r} B_j(\lambda)\ e^{-t/\tau_j} \quad (3)$$

where the amplitude spectra $B_j(\lambda)$ are defined as

$$B_j(\lambda) = \sum_i [A_i(\lambda) - A_p(\lambda)] C_{ij} \quad (4)$$

It is convenient to express eqs 1 and 4 in matrix notation

$$\Delta\mathbf{A} = (\mathbf{A} - \mathbf{A}_p)\mathbf{n} \quad (5)$$

$$\mathbf{B} = (\mathbf{A} - \mathbf{A}_p)\mathbf{C} \quad (6)$$

The row index of $\Delta\mathbf{A}$, $\mathbf{B}$, $\mathbf{A}$, and $\mathbf{A}_p$ is the wavelength λ, and the column index of $\Delta\mathbf{A}$ and $\mathbf{n}$ is the time t. The column index of $\mathbf{B}$ and $\mathbf{C}$ is the jth component. The column index of $\mathbf{A}$ and $\mathbf{A}_p$, and the row index of $\mathbf{C}$ and $\mathbf{n}$, is the ith intermediate. Matrix $\mathbf{A}_p$ consists of identical columns $\vec{A}_p$. The amplitude spectra, the columns of matrix $\mathbf{B}$, are ordered in eq 6 from low to high apparent time constants. New matrices $\tilde{\mathbf{B}}$ and $\tilde{\mathbf{C}}$ are formed from the colums of $\mathbf{B}$ and $\mathbf{C}$ by adding up columns in the following way:

$$(\tilde{\mathbf{B}})_k = \sum_{j=k}^{r} (\mathbf{B})_j;\ (\tilde{\mathbf{C}})_k = \sum_{j=k}^{r} (\mathbf{C})_j;\ k = 1, ..., r \quad (7)$$

The columns of $\tilde{\mathbf{B}}$ represent the extrapolated absorption difference spectra, and the columns of $\tilde{\mathbf{C}}$ contain the relative contributions of the intermediates in these difference spectra. In the case of PYP at alkaline pH, only three intermediates contribute as we will see: I_1, I_1', and I_2'. Their relative contributions to the ith extrapolated absorption difference spectrum will be called (x_i, y_i, z_i) in the order I_1, I_1', I_2'. Equation 6 can be rewritten in terms of $\tilde{\mathbf{B}}$ and $\tilde{\mathbf{C}}$:

$$\tilde{\mathbf{B}} = (\mathbf{A} - \mathbf{A}_p)\tilde{\mathbf{C}} \quad (8)$$

Equation 8 can be solved for $\mathbf{A}$. The intermediate spectrum $(\mathbf{A})_i$ can then be calculated from column i of matrix $\tilde{\mathbf{C}}^{-1}$:

$$(\mathbf{A})_i = \tilde{\mathbf{B}}(\tilde{\mathbf{C}}^{-1})_i + \vec{\mathbf{A}}_p \quad (9)$$

Likewise, the time courses of the intermediates *n* can be obtained by inverting eq 5 and using $\tilde{\mathbf{C}}$ and $\tilde{\mathbf{B}}$:

$$\mathbf{n} = \tilde{\mathbf{C}}(\tilde{\mathbf{B}})^{-1}\Delta\mathbf{A} \quad (10)$$

Thus, both the spectrum and time course of intermediate *i* can be obtained using eqs 9 and 10, respectively, from the amplitude spectra $B_i(\lambda)$ and knowledge of the $\tilde{\mathbf{C}}$ matrix. A unique solution for the elements of $\tilde{\mathbf{C}}$ only exists if the columns of $\tilde{\mathbf{B}}$ are linearly independent. Since there are only three linearly independent spectroscopic species that contribute significantly at alkaline pH, $\tilde{\mathbf{B}}$ contains only three columns and $\tilde{\mathbf{C}}$ is a square matrix of rank 3. To make further progress in the calculation of the elements of $\tilde{\mathbf{C}}$, the following two assumptions are used.

(1) The sum of the relative intermediate concentrations of I_1, I_1', and I_2' in the extrapolated difference spectra is constant at all times before ground-state recovery and equals the fraction of molecules cycling, η. This means that the sum of *x*, *y*, and *z* for each extrapolated difference spectrum equals η or that the sum of the matrix elements of each column of $\tilde{\mathbf{C}}$ equals η:

$$\sum_{i=1}^{3}\tilde{\mathbf{C}}_{ij} = \eta \Leftrightarrow \sum_{i=1}^{3}\tilde{\mathbf{C}}^{-1}{}_{ij} = 1/\eta; \quad j = 1, 2, 3 \quad (11)$$

This is simply the conservation law for the number of cycling molecules in a sequential cycle.

(2) The S_0-S_1 transition of the chromophore in the I_2' intermediate is blue shifted with respect to the corresponding transition in the dark state P as a consequence of the protonation of the chromophore. Therefore, the longest wavelength transition of I_2' is the UV transition at 355 nm and this is supported by quantum chemical calculations. Since the spectra of all intermediates have similar bandwidths, we can estimate from the spectrum of P, which does not absorb beyond 500 nm, that I_2' does not absorb beyond 410 nm. Our second assumption is thus that the absorption of I_2' is identical to zero for wavelengths larger than or equal to 410 nm.

Matrix calculations were performed with Matlab version R12.1. Fits with sums of exponentials were carried out with Microcal Origin version 7.5.

RESULTS

Spectra and Time Courses of Intermediates at pH 10: Extrapolated Difference Method. Panels A and B of Figure 1 allow a comparison between the transient absorption changes at pH 10 (A) and pH 6 (B) at a number of selected wavelengths. The data show striking differences between these two pH values in the time range between 200 μs and 2 ms, for wavelengths between 390 and 420 nm. We will argue that this difference at pH 10 is due to the transient formation and decay of an intermediate called I_1' which absorbs maximally around 425 nm and has rise and decay times of 330 μs and 1 ms, respectively (the first two vertical dashed lines of panel A). Comparing the trace in panel A at 340 nm (rise of the I_2' intermediate) with those at 390−420 nm, we note that the additional contribution in the latter traces develops prior to the rise of the I_2' intermediate (~1 ms). The transient absorbance changes at pH 10 were measured at 33 wavelengths, ranging from 330 to 510 nm, in the time range from 100 ns to 5 s. Only eight of these traces are shown in Figure 1A. The complete data set of 33 wavelengths from 20 μs to 5 s was subjected to SVD analysis. The first six singular values were 11.8, 2.6, 0.28, 0.071, 0.059, and 0.051. Since the contributions from s_4-s_6 are within the noise level, we consider only the first three

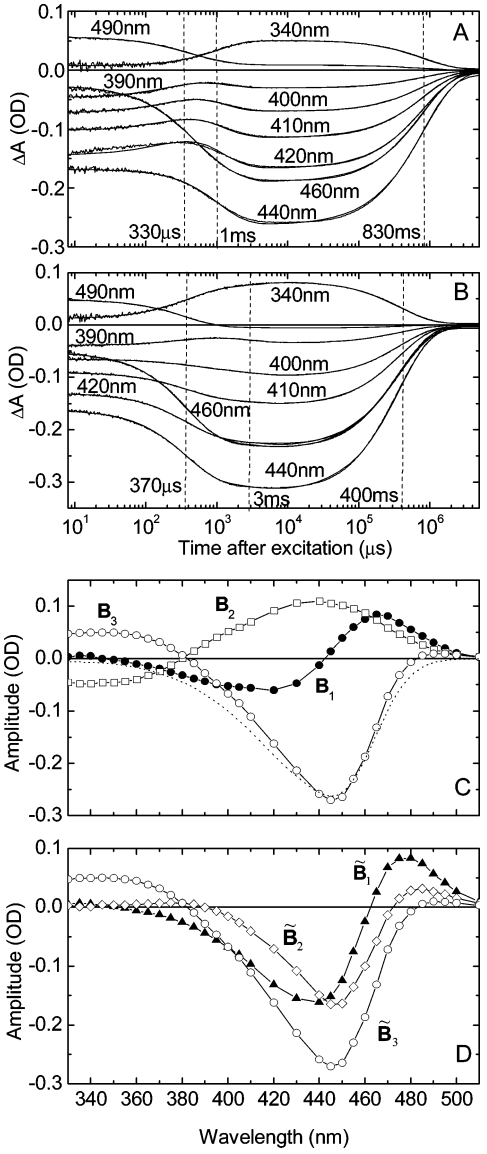

FIGURE 1: (A) Transient absorption changes after excitation at 430 nm at wavelengths varying from 330 to 510 nm. For clarity, only the traces at the indicated wavelengths are shown (eight of 33 wavelengths measured). The vertical dashed lines indicate the time constants for a global fit to the weighted SVD time traces with a sum of three exponentials. τ_1 (330 μs) is the rise time of I_1'; τ_2 (1 ms) is the rise time of I_2', and τ_3 (830 ms) is the return to P. The solid lines, only distinguishable from the data in the microsecond time range, are the fits. Conditions: pH 10, 20 °C, 50 mM KCl, and 20 mM Tris. The PYP concentration was 58 μM. (B) Corresponding data at pH 6. The PYP concentration was 43 μM (C) Amplitude spectra $B_i(\lambda)$ calculated from the amplitudes of the exponential fits to the SVD time traces and the corresponding basis spectra of the data in panel A. The three amplitude spectra correspond to the following time constants: $\tau_1 = 330$ μs (●), $\tau_2 =$ 1 ms (□), and $\tau_3 = 830$ ms (○). The dotted line is a scaled and inverted ground-state spectrum. (D) Extrapolated difference spectra obtained from the amplitude spectra of panel C according to eq 7: $\tilde{\mathbf{B}}_1$ (▲), $\tilde{\mathbf{B}}_2$ (◇), and $\tilde{\mathbf{B}}_3$ (○).

components to be significant. This suggests the presence of only three spectrally distinguishable intermediates. The three weighted time traces from SVD were fitted simultaneously starting at 8 μs with a sum of three exponentials with the following time constants: $\tau_1 = 330$ μs, $\tau_2 = 1$ ms, and $\tau_3 =$ 830 ms. The solid lines in Figure 1A represent these fit curves for the individual time traces. From the fit to the SVD time traces and the corresponding basis spectra, the amplitude spectra $B_j(\lambda)$ were calculated (*36*). These are presented in Figure 1C. The amplitude spectrum $B_1(\lambda)$ associated with the 330 μs lifetime has a positive peak near 465 nm and a negative peak near 420 nm with no contribution in the UV (350 nm). The data thus clearly show that in this transition I_1 is converted to I_1' without the formation of I_2'. This conclusion follows directly from inspection of the data [i.e., the amplitude spectrum $B_1(\lambda)$] and is model-independent. The amplitude spectrum $B_2(\lambda)$ associated with the 1 ms lifetime has a very broad positive contribution between 380 and 500 nm and a negative contribution in the UV (350 nm). $B_2(\lambda)$ thus strongly suggests that in this latter transition an I_1-I_1' equilibrium decays to I_2'. Note that the scaled ground-state spectrum in Figure 1C (⋯) does not fit to $B_3(\lambda)$ for wavelengths larger than 410 nm, indicating the presence of I_1 and I_1' in equilibrium with I_2' before recovery.

The three amplitude spectra, $\mathbf{B}_1$, $\mathbf{B}_2$, and $\mathbf{B}_3$, were used to construct the $\tilde{\mathbf{B}}$ matrix according to eq 7. The three columns, $\tilde{\mathbf{B}}_1$, $\tilde{\mathbf{B}}_2$, and $\tilde{\mathbf{B}}_3$, representing the extrapolated difference spectra are presented in Figure 1D. $\tilde{\mathbf{B}}_1$ is the initial absorbance change right after the flash and suggests that the initial bleach led to the formation of the I_1 intermediate (positive absorbance change near 480 nm). $\tilde{\mathbf{B}}_2$ is the difference spectrum with respect to the ground state after the first transition. Inspection of Figure 1D shows that below 390 nm $\tilde{\mathbf{B}}_2(\lambda)$ is zero, i.e., has no contribution from intermediates absorbing in the UV like I_2'. Inspection of $\mathbf{B}_1(\lambda)$, $\mathbf{B}_2(\lambda)$, and $\tilde{\mathbf{B}}_2(\lambda)$ thus allows the conclusion that I_1' is the direct decay product of I_1. We note that this conclusion was already evident from the experimental time traces at 390, 400, 410, and 420 nm of Figure 1A.

We now use the second constraint, that I_2' does not absorb beyond 410 nm, and consider eq 9 only in the range of $\lambda > 410$ nm; i.e., we drop the rows for the shorter wavelengths. Then the third column of the reduced matrix $\mathbf{A}$, corresponding to the spectrum of I_2', is the null vector: $(\mathbf{A})_3 = \vec{0}$. Since $(\mathbf{A})_3$ is zero, we can solve eq 9 for $(\tilde{\mathbf{C}}^{-1})_3$. In this way, we determine the third column of $\tilde{\mathbf{C}}^{-1}$. Provided that the number of wavelength points is larger than 3, eq 9 is an overdetermined system of linear equations, for which the least-squares solution may be found by multiplication with the pseudoinverse of $\tilde{\mathbf{B}}$ from the left and rearranging:

$$(\tilde{\mathbf{C}}^{-1})_3 = -(\tilde{\mathbf{B}})^{-1}\,\vec{\mathbf{A}}_p \qquad (12)$$

Using the well-established ground-state spectrum $\vec{\mathbf{A}}_p$ and the measured $\tilde{\mathbf{B}}$ spectra, we find from eq 12 for the three elements of the third column of $\tilde{\mathbf{C}}^{-1}$ values of 0.103, −4.52, and 7.56. Using the first constraint, the sum of these matrix elements equals η^{-1}. In this way, we find for the fraction of cycling molecules $\eta = 0.318$. Finally, using $\tilde{\mathbf{B}}$ and $\vec{\mathbf{A}}_p$ for the whole spectral range allows us to calculate the spectrum of I_2' from $(\tilde{\mathbf{C}}^{-1})_3$ using eq 9. The result is shown in Figure 2A (■).

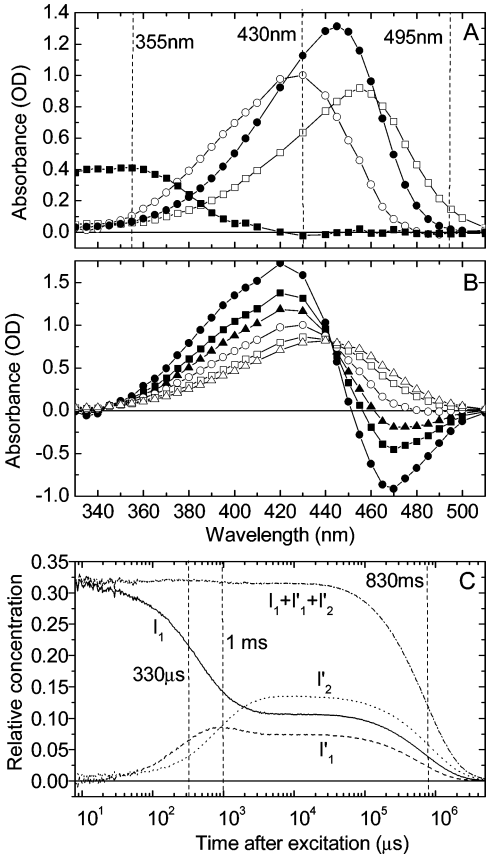

FIGURE 2: (A) Intermediate spectra of I_1 (□), I_1' (○), and I_2' (■) calculated from the extrapolated difference spectra of Figure 1D. (●) Spectrum of the dark state P for comparison. Vertical dashed lines indicate the wavelengths of the blue (430 nm), violet (355 nm), and green (495 nm) excitation flashes that were used. (B) I_1' spectra for various allowed values of y_2 as described in the text: $y_2 = 0.05$ (●), $y_2 = 0.07$ (■), $y_2 = 0.09$ (▲), $y_2 = 0.13$ (○), $y_2 = 0.21$ (□), and $y_2 = 0.3$ (△). (C) Time courses of the relative concentrations of I_1 (—), I_1' (- - -), and I_2' (⋯) calculated according to eq 10 with $y_2 = 0.13$. The time courses of the sum of the relative concentrations of I_1, I_1', and I_2' are indicated with a dotted−dashed line. The vertical dashed lines indicate the time constants from the global SVD fit of Figure 1A.

Further progress can be made by noting that only I_1 contributes to $\tilde{\mathbf{B}}_1$ (Figure 1D). Thus, the elements $\tilde{\mathbf{C}}_{21} = y_1$ and $\tilde{\mathbf{C}}_{31} = z_1$ of $\tilde{\mathbf{C}}$ are given by $y_1 = z_1 = 0$. This allows us to calculate the elements of the first column of $\tilde{\mathbf{C}}^{-1}$. The result is $\tilde{\mathbf{C}}^{-1}_{11} = 1/x_1$, $\tilde{\mathbf{C}}^{-1}_{21} = 0$, and $\tilde{\mathbf{C}}^{-1}_{31} = 0$. Since the sum of these elements equals $1/\eta$ (conservation constraint, eq 11), we have $x_1 = \eta = 0.318$. With $(\tilde{\mathbf{C}}^{-1})_1$ now completely known, we can calculate the spectrum of I_1 from $(\tilde{\mathbf{C}}^{-1})_1$, $\tilde{\mathbf{B}}$, and $\vec{\mathbf{A}}_p$ using eq 9. The result is shown in Figure 2A (□).

To calculate the spectrum of the third spectral species, I_1', we proceed in a similar fashion. From Figure 1D and as discussed above, $\tilde{\mathbf{B}}_2$ has no contribution from I_2'. Thus, $z_2 = 0$. The elements x_2, y_2, and z_2 of the second column of $\tilde{\mathbf{C}}^{-1}$ can now be expressed in terms of x_2, y_2, and η with the help of $\tilde{\mathbf{C}}^{-1}\tilde{\mathbf{C}} = \mathrm{I}$. Using the conservation constraint of eq 11, $x_2 + y_2 = \eta$, we finally obtain the following for the elements of the second column of $\tilde{\mathbf{C}}^{-1}$: $\tilde{\mathbf{C}}^{-1}_{12} = -(\eta - y_2)/(\eta y_2)$, $\tilde{\mathbf{C}}^{-1}_{22} = 1/y_2$, and $\tilde{\mathbf{C}}^{-1}_{32} = 0$. So we have now determined all elements of $\tilde{\mathbf{C}}^{-1}$; the only free parameter remaining is y_2. Since x_i, y_i, and z_i can only assume positive values and $x_2 + y_2 = \eta$, y_2 is restricted to values between 0 and η. The spectrum of I_1' can now be calculated from $(\tilde{\mathbf{C}}^{-1})_2$,

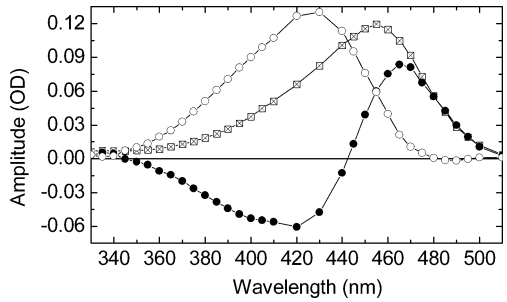

FIGURE 3: In the scaled subtraction method, the I_1 spectrum of Figure 2A is scaled down (crossed box) in such a way that its long wavelength shoulder ($\lambda \geq 485$ nm) fits optimally to the corresponding shoulder of the amplitude spectrum $B_1(\lambda)$ (●). The spectrum of I_1' (○) was obtained by subtracting the crossed box spectrum from the ● spectrum and inverting this difference.

$\tilde{\mathbf{B}}$, and $\vec{\mathbf{A}}_p$ using eq 9. The results are shown in Figure 2B for six values of y_2 from 0.05 to 0.3 ($\sim\eta$). Since the extinction coefficient has to be positive, physically meaningful absorption spectra are obtained for only $y_2 \geq 0.13$. Of the spectra for which $y_2 \geq 0.13$ in Figure 2B, we pick the one associated with $y_2 = 0.13$, since it has a spectral bandwidth which is most similar to that of the other intermediates and P. As shown in Figure 2B, for y_2 values considerably larger than 0.13, the spectral bandwidth becomes much larger than for P and I_1, which is unlikely to be correct. The spectrum of I_1' for $y_2 = 0.13$ is redrawn in Figure 2A (○). Its λ_{max} value is at ~425 nm. We note this spectrum is confirmed by an independent analysis method presented in the next section.

Since $\tilde{\mathbf{C}}$ is now completely determined (where $y_2 = 0.13$), the time courses of the intermediates may be calculated using eq 10. The time dependencies of the relative concentrations of the I_1, I_1', and I_2' intermediates are shown in Figure 2C. As expected from the data (Figure 1A), I_1 partially decays to I_1' in 330 μs. I_1 and I_1' then further decay in ~1 ms to an $I_1-I_1'-I_2'$ equilibrium. This equilibrium finally decays to P in 830 ms. Also shown is the sum of the relative concentrations of these intermediates (−•−). To a very good approximation, this sum is constant over the entire time range prior to the decay to P, as it should be. Its value is very close to $\eta = 0.318$, the fraction cycling, showing the internal consistency of the analysis.

Spectrum of I_1': Scaled Subtraction Method. The method presented in the previous section for the spectra and time courses of the intermediates is rigorous but not intuitive. We therefore present in addition a less rigorous but more transparent method which confirms that the spectrum of the I_1' intermediate presented in Figure 2A is correct.

The starting point for this procedure is the amplitude spectrum $B_1(\lambda)$ (Figure 3) for the 330 μs transition from I_1 to I_1'. We assume that this transition involves only the I_1 and I_1' intermediates. This is strongly supported by the fact that this amplitude spectrum contains a positive peak around 465 nm presumably due to I_1 and a negative peak around 420 nm presumably due to I_1' and has zero absorbance around 355 nm where I_2' absorbs. For a sequential unidirectional transition between I_1 and I_1', $B_1(\lambda)$ should equal their difference spectrum, and experimentally, this seems to be the case. This allows us to remove the contribution of I_1 from $B_1(\lambda)$, thereby obtaining the spectrum of I_1'. This procedure is shown in Figure 3. The spectrum of I_1 is scaled so that its long wavelength shoulder matches optimally with the $B_1(\lambda)$ spectrum, which assumes that I_1' does not absorb in the matching region. As we see from Figure 3, the match is excellent for $\lambda \geq 480$ nm when the spectrum of I_1 is scaled by a factor of 0.13. Therefore, the extinction coefficient of I_1' is zero beyond 480 nm. Thus, the matching criterion is equivalent to this constraint on the I_1' spectrum. Subtracting this amount of I_1 should correct completely for the I_1 contribution, leaving the I_1' spectrum, which is shown in Figure 3. This spectrum is almost identical to that of Figure 2A obtained by the matrix method. This agreement is not fortuitous, since the constraint of requiring the extinction coefficient to be zero beyond 480 nm is equivalent to the choice $y_2 = 0.13$ (see Figure 2B). Note that, as an input, we needed the correct I_1 spectrum. Moreover, the matching of $\mathbf{B}_1$ with the scaled I_1 spectrum over the wavelength range from 480 to 510 nm (six wavelength points) was done by visual inspection.

pH Dependence of Kinetics. To learn more about the nature of the transition between the neutral and alkaline pH regimes, the photocycle kinetics was measured at seven pH values (8.0, 8.5, 9.0, 9.5, 10.0, 10.5, and 11.0). With excitation at 430 nm, time traces were collected at 14 wavelengths from 370 to 500 nm in steps of 10 nm, except at pH 10.5 and 11.0 (see below). Results for selected wavelengths are shown in Figure 4. Note that the panels of Figure 4 have very different vertical scales and correspondingly different signal-to-noise ratios. The smallest pH-induced absorbance changes are at 500 nm. The initial absorbance change is almost pH-independent at every wavelength, suggesting that the amount of I_1 formed is pH-independent. At each pH, the absorbance changes at all wavelengths could be fitted simultaneously with a sum of three exponentials. The first two time constants were virtually independent of pH. The first time constant varied between 200 and 370 μs in this pH range. For the second time constant, the range was 720 μs to 1.3 ms. As we saw above, the first transition is due to the decay of I_1 to I_1' and the second transition due to the decay of the I_1-I_1' equilibrium to the $I_1-I_1'-I_2'$ equilibrium. The data of Figure 4 show that the third time constant, the return of the $I_1-I_1'-I_2'$ equilibrium to P, is strongly pH dependent, slowing with pH. The amplitudes of the time traces around 10 ms, when the $I_1-I_1'-I_2'$ equilibrium is well-established, may be used to draw conclusions about the pH dependence of the equilibrium intermediate populations. Panel A of Figure 4 shows that the I_2' population decreases with pH. From panel E, we may conclude that the fraction of molecules in I_1 in the millisecond time range increases with pH. The traces at 450 nm (panel D) indicate that the level of ground-state depletion decreases with pH, consistent with the reduced amount of I_2'. The traces at 390 and 410 nm (panels B and C) are characteristic for I_1'. Here again, the pH dependence is consistent with an increase in the I_1-I_1' equilibrium contribution and a decrease in the amount of I_2' with pH.

To obtain the time courses of the intermediates, the data at the five pH values from 8.0 to 10.0 in steps of 0.5 were measured at 14 wavelengths from 370 to 500 nm in steps of 10 nm. Since hydrolysis occurs at high pH (*37*), fewer data points were collected at pH 10.5 and 11 to reduce the measuring time. At these pH values, data were collected at only eight wavelengths from 370 to 500 nm. The spectrally superior data at the five pH values between 8 and 10 were

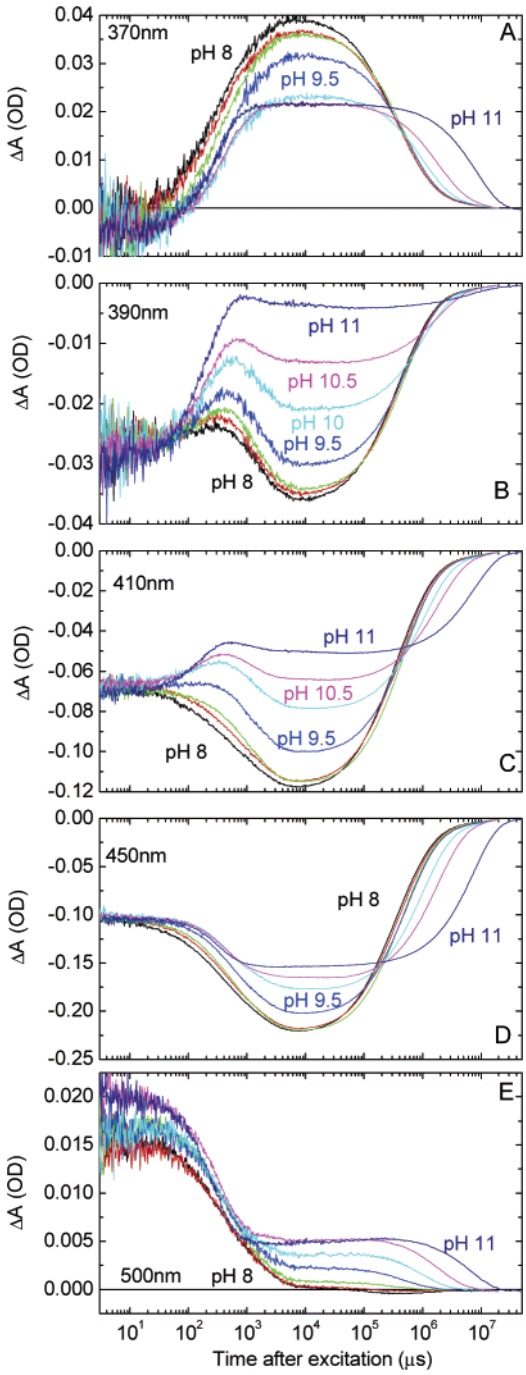

FIGURE 4: pH dependence of the transient absorbance changes after excitation at 430 nm at various wavelengths: (A) 370 nm (characteristic for I_2'), (B) 390 nm (I_2), (C) 410 nm (I_1'), (D) 450 nm (depletion signal, P), and (E) 500 nm (I_1). The color code for pH values is as follows: black for pH 8, red for pH 8.5, green for pH 9, blue for pH 9.5, light blue for pH 10, pink for pH 10.5, and dark blue for pH 11. Conditions: 20 mM Tris, 50 mM KCl, and 20 °C. The PYP concentration was 58 μM.

subjected to a joint SVD analysis, which assumed that the same spectral species contribute over the whole pH range. We then have

$$(\Delta\mathbf{A}_{pH8}, ..., \Delta\mathbf{A}_{pH10}) = \mathbf{U}^T\mathbf{D}\ (s)\ (\mathbf{V}_{pH8}, ..., \mathbf{V}_{pH10}) \quad (13)$$

The first five singular values were 17.03, 2.54, 0.45, 0.16, and 0.12. Since the contributions from s_4 and s_5 are within the noise level, we consider only the first three components to be significant. This suggests again the presence of only three spectral components, presumably, I_1, I_1', and I_2'. The time traces of the three SVD components V_i at pH 10 (where significant amounts of I_1' and I_1 are present), weighted with the corresponding singular values s_i, were fitted simultaneously with a sum of three exponentials. From the amplitudes of this fit and the basis spectra U_i, the three amplitude spectra $B_j(\lambda)$ were calculated as described previously (*36*). Finally, the extrapolated difference method was used to calculate the spectra of the intermediates (I_1, I_1', and I_2') from these amplitude spectra. The spectra of I_1, I_1', and I_2' obtained in this way (not shown) are, as expected, very similar to those from the separate measurements at pH 10 (Figure 2A), but they have the advantage that they are the best average spectra over this whole pH range. The time courses of the intermediate concentrations $n_i(t)$ at each pH were then calculated from $\Delta A(\lambda,t)$ at all 14 wavelengths and the intermediate spectra by matrix inversion of eq 5. For pH values of 10.5 and 11.0, where data at only eight wavelength values were collected, which were not included in the joint SVD, the same intermediate spectra were used to calculate their time courses, again from eq 5.

The resulting time traces are shown in Figure 5. The fractions of the molecules in I_1, I_1', and I_2' have the time dependence we expect from the data and from our previous results at pH 10 (Figure 2C). The sum of the fractions is plotted in Figure 5D. This sum is practically constant in time until the ground-state recovery, as required. Moreover, this plateau value is virtually pH independent and equal to the fraction cycling which is similar to that of the previous experiments at pH 10 (Figure 2C). The pH dependence of the time traces in panels A−C not only confirms what was already suggested by the data at various wavelengths (Figure 4) but allows a quantitative analysis of the pH dependence of the intermediate equilibria. From around 5 ms to the ground-state recovery, the intermediate concentrations are constant in time and the intermediates are in equilibrium. The fractions in equilibrium are clearly pH dependent. The main effect is that the fraction in I_1' increases with pH at the expense of I_2'. The increase in the amount of I_1 is smaller. The population values at 10 ms (vertical dashed lines in panels A−C of Figure 5) were used as a measure for the equilibrium values. The pH dependence of the equilibrium values of the intermediate concentrations at 10 ms is plotted in Figure 6. The dotted curves are simultaneous fits of the data of panels A−C with the Henderson−Hasselbalch equation with a pK_a of 9.9 and an n of 0.96. The solid curves are individual fits with the Henderson−Hasselbalch equation. The fit parameters are as follows: I_1, pK_a = 9.3 and n = 1.21; I_1', pK_a = 10.0 and n = 0.9; and I_2', pK_a = 9.8 and n = 1.06. The global fit is excellent for I_2' and I_1', but only adequate for I_1. Panel D of Figure 6 shows the pH dependence of the rate constant for the recovery to the ground state P. This sigmoidal curve yielded a pK_a of 9.7 and a Hill coefficient of 0.87. The high-pH end value for this fit was fixed at zero.

From Figure 6, we conclude that the populations of I_1 and I_1' increase with pH, whereas the population of I_2' simultaneously decreases. One possible scheme (Scheme 1), which can explain the observed common pH dependence of the equilibrium populations and the recovery rate (Figure 6D), involves a rapid equilibrium between I_1, I_1', and I_2'. Rapid

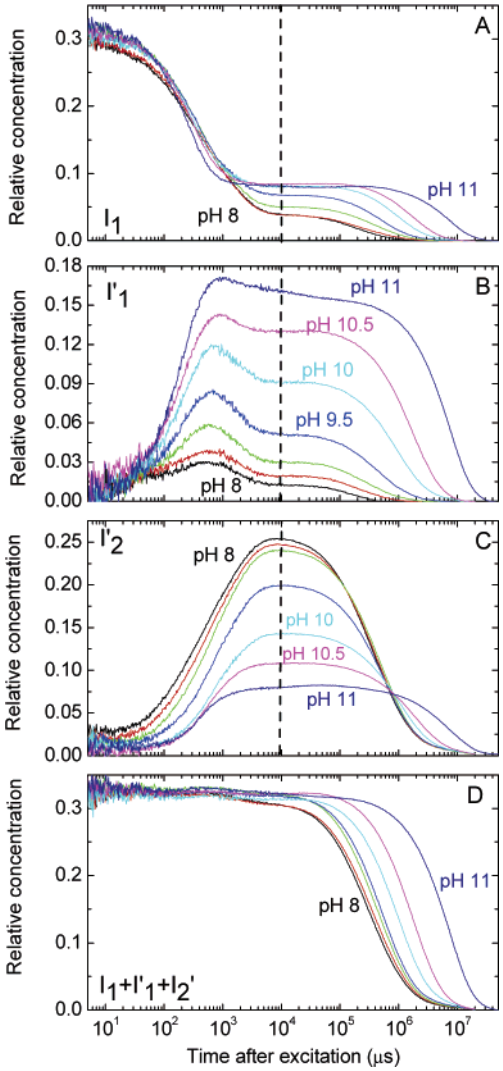

FIGURE 5: Time courses of the relative concentrations of the I_1 (A), I_1' (B), and I_2' (C) intermediates at various pH values calculated from the combined SVD values as explained in the text. (D) Time course of the sum of the populations of I_1, I_1', and I_2'. The color code is as in Figure 4.

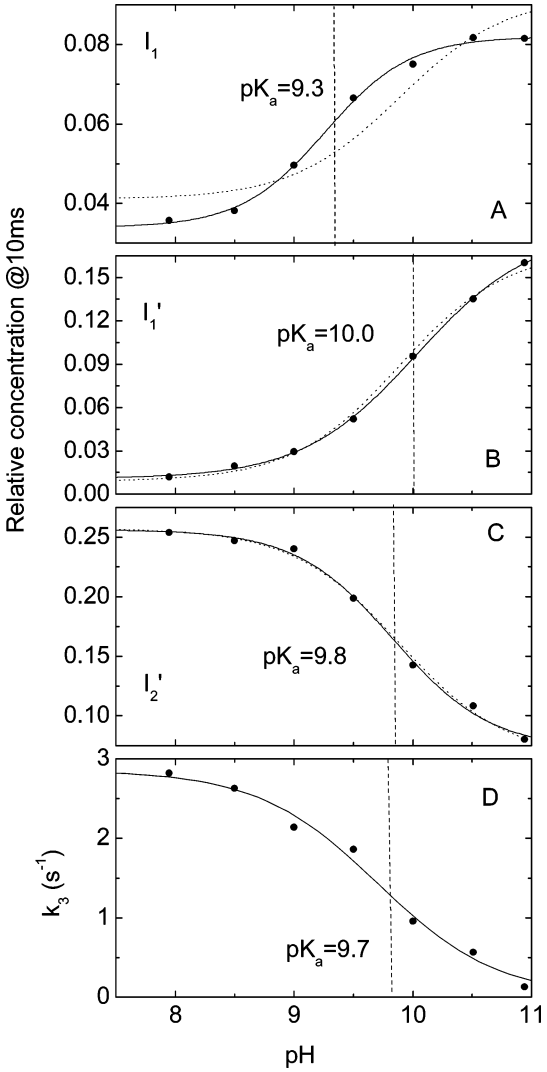

FIGURE 6: pH dependence of the equilibrium concentrations of the I_1, I_1', and I_2' intermediates at 10 ms, derived from panels A−C of Figure 5, respectively. The dotted curves are simultaneous fits of these titration curves with a pK_a of ∼9.9 and an n of ∼0.96. The solid curves are individual fits to the Henderson−Hasselbalch equation: (A) I_1, pK_a = 9.3, n = 1.21; (B) I_1', pK_a = 10.0, n = 0.9; (C) I_2', pK_a = 9.8, n = 1.06. (D) pH dependence of the k_3 decay rate for the ground-state recovery. The solid curve is a fit with the Henderson−Hasselbalch equation and a pK_a of 9.7 and an n of 0.87.

means that the equilibration rates among I_1, I_1', and I_2' are fast with respect to recovery rates k', k'', and k''' (see Scheme 1 below). The I_1−I_1' equilibrium is assumed to be pH-independent; this guarantees that the populations of I_1 and I_1' increase in parallel. The I_1'−I_2' equilibrium is pH-dependent, and the rate constants for the return to P are pH-independent.

Analysis of this reaction scheme shows that the apparent rate constant for the ground-state recovery (k_3 of Figure 6D) has the observed sigmoidal pH dependence with the highest rate at pH 8 and equal to k', and a pK_a equal to that for the I_1'−I_2' equilibrium. The observed pH dependence of the recovery rate is thus a consequence of the pH dependence of the intermediate equilibria. The data in Figure 6D with k_3 being almost zero at pH 11 suggest that $k' \gg k''$ and k'''. Since the protonation of the chromophore changes in this equilibrium, the simplest interpretation is that this pK_a of ∼9.9 represents the surface-exposed chromophore. The I_1' intermediate thus appears to be the alkaline form of I_2'.

Dependence on Delay and Wavelength of Photoreversal from I_2'. The kinetics of the photoreversal from I_2' at alkaline pH were investigated with an initial blue flash (430 nm) to

Scheme 1

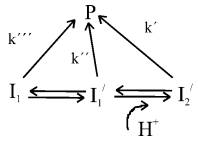

start the cycle, followed by a second violet flash [355 nm, selective for I_2'; I_1' and I_1 absorb to a much smaller extent at this wavelength (see Figure 2A)] after a variable time delay. To construct the photoreversal signal, three time traces are required: DFTV (double flash with data acquisition triggered on violet flash), BFTV (blue flash with data acquisition triggered on violet flash), and VFTV (violet flash with data acquisition triggered on violet flash). The pure photoreversal signal was calculated from these traces as described previously (*30*, *39*). The double-flash signal DFTV has to be corrected for two effects: the contribution from

those molecules that were not excited by the first, blue flash but by the second, violet flash. For this correction, we need to know f_1, the fraction of the initial PYP population that was not excited by the first flash and remains in the ground state. To obtain the true photoreversal signal, the double-flash absorbance change DFTV also has to be corrected for the contribution from those molecules cycling that are not excited by the second flash and thus complete the thermal cycle. For this correction, we need to know f_2, the fraction of cycling PYP molecules not excited by the second flash. The photoreversal signal is then constructed according to eq 2 of ref *30* from the DFTV, VFTV, and BFTV traces and the f_1 and f_2 factors.

The photoreversal signals at pH 10 were measured at 365 and 450 nm at 19 delays ranging from 500 ns to 5 s. A selection of six of these traces at each wavelength is shown in Figure 7A. The solid lines are from a two-exponential global fit to the data at all 19 delays. The data clearly show the presence of two phases with the following exponential decay constants identified by the dashed vertical lines: $\tau_1 = 60$ μs and $\tau_2 = 3.5$ ms. The corresponding amplitudes A_1 (60 μs component) and A_2 (3.5 ms) are plotted as a function of the delay in Figure 7B. The positive amplitudes refer to the photoreversal signal at 365 nm and the negative amplitudes to the signal at 450 nm. The solid lines in Figure 7B are simultaneous fits to the delay dependence of the amplitudes with a sum of two exponentials. The optimal fit was obtained with exponential time constants of 1.1 ms (rise) and 680 ms (decay). The 1.1 ms rise time corresponds closely with the 1 ms rise time of I_2' (Figure 1A). In view of the small number of delay times, the 680 ms decay time agrees well with the 830 ms decay time of I_2' (Figure 1A). The delay dependence of A_1 and A_2 in Figure 7B thus closely matches the time course of the I_2' intermediate (Figure 2C). The slow millisecond component A_2 has a much smaller amplitude than A_1 ($\sim$40%).

To characterize the spectral intermediates involved in photoreversal, its kinetics were measured at 30 wavelengths from 330 to 510 nm at the fixed delay of 10 ms (where the photoreversal amplitude is maximal). The time traces at seven selected wavelengths are shown in Figure 7C. The solid lines are from a simultaneous fit to all 30 traces with two exponentials. The two exponential time constants ($\tau_1 = 60$ μs and $\tau_2 = 2.3$ ms) are identified by vertical dashed lines in Figure 7C. The agreement with the delay data (panel A) is excellent. The corresponding amplitude spectra $B_1(\lambda)$ (red circles) and $B_2(\lambda)$ (■) associated with these two exponentials are plotted in Figure 7D. The sum of $B_1(\lambda)$ and $B_2(\lambda)$ (empty red squares) is also plotted. This sum equals the initial absorbance change after the second flash with respect to the initial dark state P.

The fact that both A_1 and A_2 have the same delay dependence and rise and decay in parallel with I_2' suggests that at alkaline pH photoreversal proceeds via $I_2'^{cis}$ under our experimental conditions. From Figure 2A, we note that the extinction coefficient of I_1' at 355 nm is only approximately one-fourth of that of I_2'. According to Figure 2C, the relative concentration of I_1' is only approximately one-half of that of I_2' with a delay of 10 ms. Together, these factors lead to an expected photoreversal signal from I_1' below the detection limit. Similar arguments hold for I_1. As shown in Figure 7D, the initial absorbance change (empty red squares) fits reasonably well with the scaled ($I_2'^{cis} - P$) difference spectrum (empty blue triangles; *30*) for wavelengths larger than 440 nm. Below 440 nm, however, significant systematic deviations are apparent. Around 345 nm, this difference is presumably due to the higher extinction coefficient of $I_2'^{trans}$ with respect to $I_2'^{cis}$ (*30*). The positive discrepancy in the range of 390−440 nm is most likely due to a contribution from the I_1' intermediate. This suggests that the second flash initially produces $I_2'^{trans}$ from which some $I_1'^{trans}$ is generated before the start of the data acquisition. This I_1' contribution could arise from rapid equilibrium with $I_2'^{trans}$ after reisomerization. Comparison of $B_1(\lambda)$ with the scaled spectrum of P (Figure 7D) indicates that, in the fast component, an I_2-like intermediate ($I_2'^{trans}$) decays and an I_1-like intermediate rises (negative mismatch near 490 nm). This transition is probably associated with proton release from the chromophore. The fact that at pH 10 it is accelerated (60 μs) with respect to pH 6 (380 μs) is consistent with faster deprotonation at the higher pH. The $B_2(\lambda)$ spectrum shows that in the subsequent slow transition the $I_1^{trans}-I_1'^{trans}$ equilibrium decays to P. This is supported by the positive contributions to B_2 around 390 nm (I_1') and 480 nm (I_1). The photoreversal transition from $I_2'^{cis}$ to P consists of three sequential steps: rapid unresolved isomerization of $I_2'^{cis}$ and formation of an $I_2'^{trans}-I_1'^{trans}$ equilibrium, the 60 μs transition from the $I_2'^{trans}-I_1'^{trans}$ to $I_1'^{trans}-I_1^{trans}$ equilibrium (chromophore deprotonation), and the return to P in $\sim$3 ms. The proposed reaction scheme is shown in Figure 8.

When these results at pH 10 are compared with our previous results at pH 6, striking differences are apparent. At pH 10, the two time constants are more widely separated and τ_2 is increased by a factor of $\sim$10 (58 and 380 μs at pH 6; 60 μs and 3.5 ms at pH 10). The dependence of both amplitudes A_1 and A_2 on the delay is the same at pH 10 and requires only two exponential time constants, 1.1 and 680 ms, which closely match the rise and decay times of I_2', respectively. At pH 6, the delay dependencies of A_1 and A_2 were very different, requiring three exponentials and suggesting photoreversal from sequential I_2 and I_2' intermediates. Moreover they showed that I_2 and I_2' are in equilibrium. In contrast to the case at pH 6, the slow millisecond component A_2 has a smaller amplitude than A_1 ($\sim$40%). Whereas both amplitude spectra at pH 6 had only contributions in the 330−380 nm region from I_2 and I_2' intermediates, at pH 10 B_1 has a spectrum corresponding to I_2 or I_2', but B_2 has contributions from I_1' and I_1. The data at pH 10 provide no evidence for a sequential I_2 to I_2' step or for an I_2-I_2' equilibrium. We conclude that at pH 10 very little or no I_2 remains. At this pH, there is only one intermediate with a protonated chromophore, I_2', and I_1' and I_2' are in equilibrium.

Using a second green flash (495 nm) and a delay of 20 μs, we detected efficient photoreversal from I_1 at pH 10, with a time constant for the return to P of <1 μs (data not shown). This result is the same as that previously obtained at pH 6 (*30*).

DISCUSSION

The kinetics of the photocycle and photoreversal of PYP were investigated at alkaline pH. We find that the intermediate I_1' that forms above pH 9 is the decay product of I_1. Evidence for this intermediate was also obtained from the

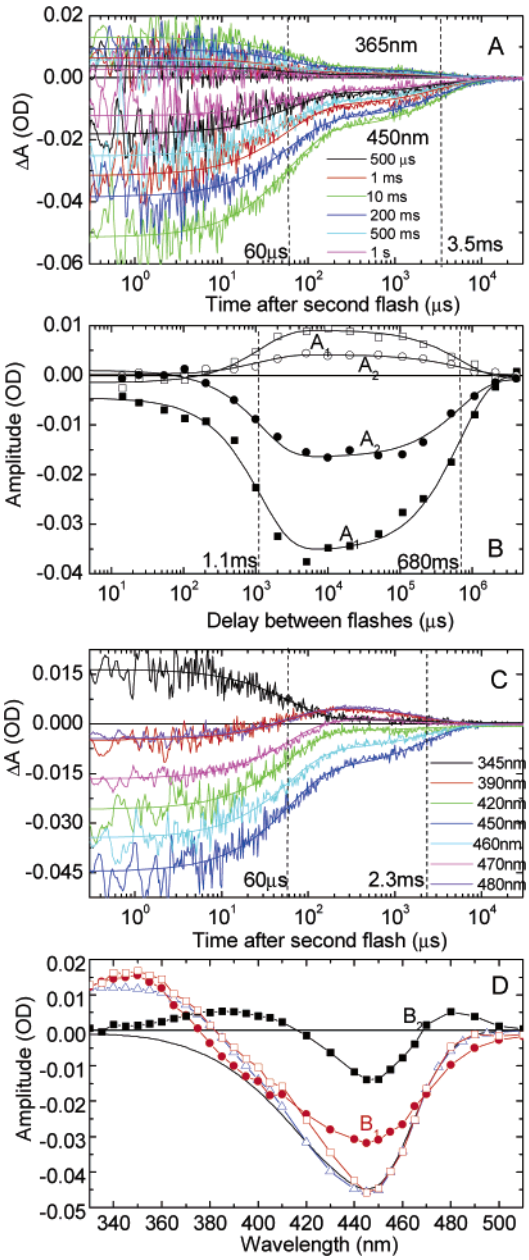

FIGURE 7: (A) Photoreversal signals, at 365 and 450 nm, at six delays ranging from 500 μs to 1 s (first flash at 430 nm, second flash at 355 nm). For clarity, the data at 13 other delays are not shown. The solid lines represent a two-exponential global fit to all of the data with a τ_1 of 60 μs and a τ_2 of 3.5 ms marked by the dashed vertical lines. Conditions: pH 10, 20 °C, 50 mM KCl, and 20 mM Tris. The PYP concentration was 58 μM. (B) Dependence of the photoreversal amplitudes A_1 and A_2 on the delay. A_1 and A_2 are the amplitudes of the fast (60 μs) and slow (3.5 ms) components, respectively, obtained from the global fit of the delay data of panel A. The two positive amplitudes [□ (A_1) and ○ (A_2)] are for the data at 365 nm; the two negative amplitudes [■ (A_1) and ● (A_2)] are for the data at 450 nm. The vertical dashed lines at 1.1 and 680 ms indicate the values of the time constants for a global fit with two exponentials. The solid curves represent the fit. (C) Photoreversal signals at seven wavelengths between 330 and 510 nm at the fixed delay of 10 ms. For clarity, similar data at 23 additional wavelengths are not shown. The solid lines are the global fits with a sum of two exponentials with the common time constants τ_1 (60 μs) and τ_2 (2.3 ms) marked by the vertical dashed lines. (D) Amplitude spectra $B_1(\lambda)$ and $B_2(\lambda)$ associated with τ_1 and τ_2 obtained from the global fit of (B): B_1 (filled red circles), B_2 (■), sum of B_1 and B_2 (empty red squares), and down scaled $I_2'^{cis}$ − P difference spectrum (empty blue triangles). The solid black curve is a scaled P spectrum.

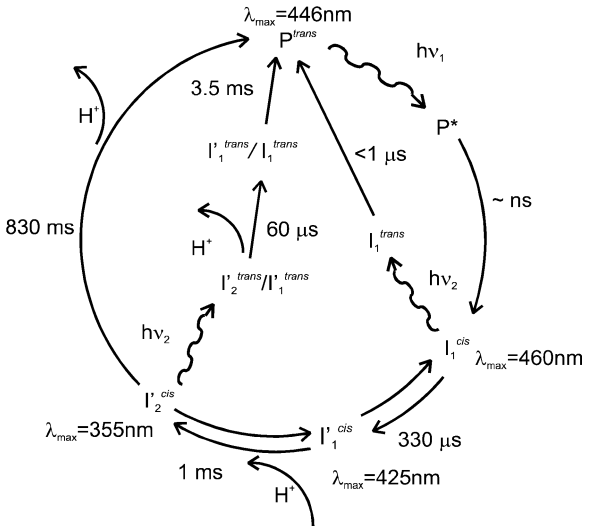

FIGURE 8: Proposed model for the kinetics of the photocycle and photoreversal of PYP at pH 10. Note the equilibria among I_1, I_1', and I_2'. These three intermediates decay together to P. For clarity, the short-lived intermediates I_0 and $I_0^{\ddagger}$ between P* and I_1 are not shown.

B_1 and B_2 amplitude spectra of the photoreversal kinetics. Recently, we also detected an I_1'-like intermediate at alkaline pH in the Y98Q mutant (*25*). The spectrum of I_1' has its maximum at ~425 nm, between the λ_{max} values of I_1 and I_2'. At neutral pH, three intermediates are required, in the sequence I_1, I_2, and I_2'. In I_2', the chromophore is believed to be exposed and protonated. Since at sufficiently high pH the exposed chromophore can no longer be protonated, the I_1' intermediate may be regarded as the alkaline form of I_2' with a deprotonated chromophore but a similar structure. Indeed, a wavelength maximum of 425 nm is consistent with a deprotonated partially exposed chromophore. For both the cis and trans forms, a shift of ~58 nm is observed between the λ_{max} values of the protonated and deprotonated bound exposed chromophore (*27*). The electronic spectra of I_2 and I_2' at pH 7 can be distinguished, and the λ_{max} values for I_2 and I_2' are ~370 and ~350 nm, respectively (*12*; B. Borucki et al., manuscript to be published). Thus, the deprotonated forms of I_2 and I_2' may be expected to have their λ_{max} values near 430 and 410 nm, respectively. The observed value of 425 nm is therefore reasonable, and it seems likely that I_1' has a deprotonated chromophore. This question could be settled by time-resolved vibrational spectroscopy.

With regard to the intermediate nomenclature, we labeled the 425 nm alkaline species, I_1'. The subscript 1 was chosen since its chromophore is deprotonated, and a prime was added to distinguish it from its precursor, I_1. We note that for the wild type at neutral pH, heterogeneity in I_1 has been detected by FTIR (*17*), resonance Raman (*40*), and X-ray diffraction (*5*). In those cases, the I_1-like intermediates had chromophores that were still hydrogen bonded in the binding pocket, whereas I_1' at alkaline pH refers most likely to a state with a surface-exposed chromophore. For the E46Q mutant, we previously introduced an intermediate I_1' between I_1 and I_2 which had a surface-exposed chromophore and was in a pH-dependent equilibrium with I_2 (*24*). In that case, we had no evidence, however, that this intermediate absorbed at 425 nm in the pH range that was studied.

Our results for the photocycle showed that at pH 10, I_1 decays partially to I_1' (330 μs). I_1 and I_1' then decay further

to I_2' (1 ms). The $I_1-I_1'-I_2'$ equilibrium finally decays to P in 830 ms. The proposed reaction scheme for the kinetics of the photocycle and the photoreversal at pH 10 is presented in Figure 8.

The spectra of I_1, I_2', and I_1' (Figure 2A) as well as their time courses were obtained from the transient absorbance data with the help of the extrapolated difference method (*31*). The assumptions used in this procedure are plausible and explained in detail in Materials and Methods: (1) the absorbance of I_2' is zero beyond 410 nm, and (2) the sum of the relative intermediate contributions to the extrapolated difference spectra is constant and equals the fraction cycling. This method was previously successful with bacteriorhodopsin where in addition constraints from linear dichroism were used (*31*). It is validated for PYP by the fact that the spectra of I_2' and I_1 are in excellent agreement with previous work (*30*), that the sum of the relative intermediate concentrations remains constant during the cycle until the recovery of the ground state (Figure 2C), and that an independent analysis (scaled subtraction) led to the same spectrum for I_1'.

The spectrum of the UV intermediate in Figure 2A was assigned to I_2' and not to I_2, since its wavelength maximum is at 355 nm. The spectra of I_2 and I_2' are known to have their maxima at ~370 and ~350 nm, respectively (*12*; B. Borucki et al., manuscript to be published). At neutral pH, the I_2 and I_2' intermediates are in equilibrium (*30*). This equilibrium is pH-dependent with a pK_a of 6.2 (*12*; B. Borucki et al., manuscript to be published). Above this pK_a, the I_2' intermediate dominates (*12*; B. Borucki et al., manuscript to be published). At alkaline pH, we therefore expect to observe only I_2'. The absence of an I_2 intermediate at alkaline pH is furthermore supported by the photoreversal experiments which indicate the presence of only one I_2-I_2'-like intermediate.

We confirmed the result for the I_1' spectrum by an alternative less accurate and more subjective method. This scaled subtraction method has an advantage in that it is easier to understand. It requires as input an accurate I_1 spectrum, and the result depends on this choice. Moreover, the visual scaling procedure is inaccurate. We used the amplitude spectrum $\mathbf{B}_1$ for the rise of I_1' (330 μs) in this procedure (see Figure 3). The agreement with the spectrum of I_1' from the extrapolated difference method was excellent. The amplitude spectra $\mathbf{B}_2$ (1 ms) or $\mathbf{B}_3$ (830 ms) may also be used to extract the I_1' spectrum but lead to increasingly inaccurate results. Using $\mathbf{B}_2$ requires accurate input spectra of I_1 and I_2'. Using $\mathbf{B}_3$ requires all three spectra of I_1, I_2', and P. Repeated successive scaling and multiple subtraction steps lead to an accumulation of errors. The extrapolated difference method is superior, since it takes into account all three amplitude spectra.

In previous work, approximate spectra for I_1' were obtained from photostationary light−dark difference spectra at alkaline pH (*11*, *27*, *29*). These spectra have to be corrected for the contributions from other intermediates (I_1 and I_2') that accumulate at high pH under background illumination. Such measurements suffer moreover from potential artifacts due to the efficient photoreversal of these intermediates (e.g., I_1) by the background illumination. Due to the very slow recovery rates at alkaline pH, this correction is essential. The first spectrum determined in this way had only six wavelength points and a λ_{max} value of ~420 nm (*29*). More recently (*27*), a spectrum was presented for PYP_M^{410}, which has a λ_{max} value of 410 nm and an extinction coefficient that is only half as large as ours. In ref *27*, a version of the scaled subtraction method was applied to $\mathbf{B}_3$. The large differences with our results may be due to the problems with that method, as described in the previous section. In ref *11*, spectra of an intermediate pB^{deprot} with a λ_{max} of ~430 nm were obtained with a diode array spectrometer. Our spectra for I_1' were obtained from the wavelength dependence of the transient absorption data and do not suffer from the problems described above.

Our measurements provide for the first time kinetic information about the formation of the I_1' intermediate. The amplitude spectrum $B_1(\lambda)$ (Figure 1C), which is derived directly from the data without any assumptions, clearly proves that in the 330 μs transition I_1 decays to I_1', without the formation of I_2'. $B_2(\lambda)$ shows that in the next transition I_1 and I_1' decay to I_2'. These results are model-independent. Further analysis, based on the extrapolated difference method and a few plausible assumptions, confirms these results. Both the time traces (Figure 1A) and the intermediate time courses (Figure 2C) derived from these data indicate that I_1' is the decay product of I_1 and decays in equilibrium with I_1 and I_2' to P. In ref *11*, the intermediate pB^{deprot} (equivalent to I_1') was introduced between I_2' and P, and in equilibrium with I_2'. It was concluded that pB^{deprot} (I_1') is the decay product of pB (I_2'). Our kinetic data prove that this is incorrect and that I_1' is formed from I_1. The photocycle model in Figure 4 of ref *11* is thus also incorrect.

Assuming that the spectra of I_1, I_1', and I_2' are pH-independent and that no other intermediates contribute, we inverted eq 5 to calculate the time traces of these intermediates at each pH. We then used the stationary equilibrium values at 10 ms to derive titration curves for the I_1, I_1', and I_2' populations (Figure 6). The results show that with increasing pH the equilibrium concentrations of I_1 and I_1' in the millisecond time range increase at the expense of a corresponding decrease in the I_2' concentration. The common pK_a is ~9.9. The pH dependence of the rate constant for the return to the ground state from this equilibrium was sigmoidal with a pK_a of ~9.7 (Figure 6D), within experimental error equal to the value of the pK_a for the pH-dependent change in equilibrium populations. These data were analyzed on the basis of Scheme 1, in which only the $I_1'-I_2'$ equilibrium is pH-dependent. We find that the pH dependence of the recovery rate is a consequence of the corresponding pH dependence of the $I_1'-I_2'$ equilibrium. We attribute the pK_a of 9.9 to the phenol group of the partially exposed chromophore, in agreement with previous assignments (*37*, *38*).

We analyzed our data on the basis of the simple kinetic Scheme 1 with only one pK_a. The titration of Figure 6 suggested the presence of a common pK_a of ~9.9. We attributed the poor fit for I_1 (with an individual pK_a of ~9.3; Figure 6A) to experimental error (low signal-to-noise ratio) and the very limited number of pH points. The pH dependence of the equilibrium populations (Figure 6) is based on the time traces of Figure 5. These depend in turn on the intermediate spectra. We noted that some residual freedom remained in these spectra (value of the parameter y_2), which leads to corresponding uncertainty in the time traces and pH dependencies. For these reasons, we do not want to overin-

terpret our data and thus limit our analysis to one common pK_a. The possibility that the pK_a of 9.3 is real and that there are two very close pK_a values cannot be excluded. This would require a more complex kinetic scheme, such as that discussed for the Y98Q mutant (*25*).

It has long been known that the rate constant for the ground-state recovery has a bell-shaped pH dependence with pK_a values of 6.4 and 9.4 (*23*, *38*). In ref *38*, these data were analyzed on the basis of an equilibrium model implying that the recovery of P proceeds via a species with a deprotonated chromophore and protonated Glu46, i.e., an I_1-like species. Since the microscopic rate for the transition from this I_1-like state to P was assumed to be pH-independent (*38*), the apparent rate constant of the recovery of P follows the accumulation of the I_1-like state in the equilibrium that is maximal at pH ~8.0. We note that no amplitude data were used in this analysis to confirm the assumed accumulation of the I_1-like state. Here we show that the accumulation of I_1 in the equilibrium increases from pH 8 to 10, which is inconsistent with the proposed model (*38*). Moreover, we provide an explanation for the higher pK_a in terms of the pH dependence of the $I_1'-I_2'$ equilibrium.

We determined the equilibrium concentrations of intermediates I_1, I_1', and I_2' from their time courses and provided direct kinetic evidence for the existence of their equilibria. In ref *24*, we first demonstrated the equilibrium between I_1 and I_2' at pH 11. Recently, the equilibrium concentrations of these intermediates at alkaline pH were obtained from photostationary absorption spectra in the presence of background illumination (*27*). The pH dependencies of $I_1'$and I_2' agree fairly well with our results. A pK_a of 10.2 was obtained for this equilibrium, in good agreement with our value of 9.9. The results for I_1 disagree, however. According to ref *27*, the fraction of molecules in I_1 rises with pH up to pH 10.2 and then decreases again. Our data points (Figure 6A) agree up to pH 10 but do not decrease at higher pH values. We showed recently that the ionic strength also affects these equilibria (25), with an increasing salt concentration shifting the I_1-I_1' equilibrium toward I_2'. Differences in the amounts of salt added during the titration may thus explain the discrepancy. The steady-state data in ref *27* were collected under continuous illumination using light with wavelengths above 430 nm. Another contribution to the discrepancy could thus be photoreversal from I_1 ($\lambda_{max} \sim 460$ nm), which would reduce the I_1 population, in particular, at the highest pH values where the return to the initial state is slowest.

On the basis of these data, two very close pK_a values were introduced in ref *27*. The first one (10.2) was assigned to the $I_2'-I_1'$ equilibrium, as discussed. The second one (10.4) was assigned to the I_1-I_2' equilibrium. We note that this assignment is inconsistent since the two distinct pK_a values refer to the protonation of the chromophore, i.e., to only one protonatable group. However, the finding of two pK_a values requires the involvement of two protonatable groups. Consequently, one of the two pK_a values of ref *27* reflects the protonation of a residue that occurs in an equilibrium between I_1 and I_1', which both have a deprotonated chromophore. In Scheme 1, which can explain both the equilibrium and kinetic data of Figure 6, we have only one pH-dependent equilibrium between I_1' and I_2', and the I_1-I_1' equilibrium is pH-independent.

Our results for photoreversal with the second flash at 355 nm are very different at pH 10 and 6. At pH 6, we observed photoreversal from two sequential intermediates, I_2 and I_2', that were in equilibrium and had their own photoreversal time (58 and 380 μs for I_2 and I_2', respectively). At pH 10, there is only one intermediate with a protonated chromophore, I_2'. The photoreversal kinetics again have two phases (60 μs and 3.5/2.3 ms). However, their interpretation is very different. The first unresolved step is again the rapid isomerization from $I_2'^{cis}$ to $I_2'^{trans}$. Some $I_1'^{trans}$ is also already present ~100 ns after the second flash, possibly from rapid equilibration with $I_2'^{trans}$. In the 60 μs phase, $I_2'^{trans}$ decays to I_1^{trans}. This transition is associated with chromophore deprotonation. In the next, slower phase (3.5 ms), I_1^{trans} and $I_1'^{trans}$ decay to P. The associated amplitude spectrum B_2 provides clear evidence for the participation of I_1- and I_1'-like intermediates in the photoreversal. The photoreversal results thus provide further support for the existence of the I_1' intermediate at alkaline pH.

CONCLUSIONS

Using transient absorption spectroscopy, we determined the spectra and time courses of the three intermediates (I_1, I_1', and I_2') that play a role in the photocycle above pH 8. I_1' has its absorption maximum at 425 nm and is the decay product of I_1. Beyond 1 ms, the three intermediates are in equilibrium. Assuming that their spectra are pH-independent, we determined the pH dependence of their time courses. This allowed the determination of a pK_a of ~9.9 between I_1' and I_2', which is assigned to the deprotonation of the exposed chromophore. The existence of the I_1' intermediate and the absence of the I_2 intermediate at alkaline pH are supported by photoreversal measurements.

REFERENCES

1. Cusanovich, M. A., and Meyer, T. E. (2003) Photoactive yellow protein: A prototypic PAS domain sensory protein and development of a common signaling mechanism, *Biochemistry 42*, 4759−4770.
2. Hellingwerf, K. J., Hendriks, J., and Gensch, T. (2003) Photoactive yellow protein, a new type of photoreceptor protein: Will this "yellow lab" bring us where we want to go? *J. Phys. Chem. A 107*, 1082−1094.
3. Borgstahl, G. E. O., Williams, D. R., and Getzoff, E. D. (1995) 1.4 Å structure of photoactive yellow protein, a cytosolic photoreceptor: Unusual fold, active site and chromophore, *Biochemistry 34*, 6278−6287.
4. Rajagopal, S., Anderson, S., Šrajer, V., Schmidt, M., Pahl, R., and Moffat, K. (2005) A structural pathway for signalling in the E46Q mutant of photoactive yellow protein, *Structure 13*, 55−63.
5. Ihee, H., Rajagopal, S., Šrajer, V., Pahl, R., Anderson, S., Schmidt, M., Schotte, F., Anfinrud, P. A., Wulff, M., and Moffat, K. (2005) Visualizing reaction pathways in photoactive yellow protein from nanoseconds to seconds, *Proc. Natl. Acad. Sci. U.S.A. 102*, 7145−7150.
6. Genick, U. K., Borgstahl, G. E., Ng, K., Ren, Z., Pradervand, C., Burke, P. M., Srajer, V., Teng, T. Y., Schildkamp, W., McRee, D. E., Moffat, K., and Getzoff, E. D. (1997) Structure of a protein photocycle intermediate by millisecond time-resolved crystallography, *Science 275*, 1471−1475.
7. Dux, P., Rubinstenn, G., Vuister, G. W., Boelens, R., Mulder, F. A. A., Hard, K., Hoff, W. D., Kroon, A. R., Crielaard, W., Hellingwerf, K. J., and Kaptein, R. (1998) Solution structure and backbone dynamics of the photoactive yellow protein, *Biochemistry 37*, 12689−12699.

8. Taylor, B. L., and Zhulin, I. B. (1999) PAS domains: Internal sensors of oxygen, redox potential, and light, *Microbiol. Mol. Biol. Rev. 63*, 479−506.
9. Hoff, W. D., van Stokkum, I. H. M., van Ramesdonk, H.-J., van Brederode, M. E., Brouwer, A. M., Fitch, J. C., Meyer, T. E., van Grondelle, R., and Hellingwerf, K. J. (1994) Measurement and global analysis of the absorbance changes in the photocycle of the photoactive yellow protein from *Ectothiorhodospira halophila*, *Biophys. J. 67*, 1691−1705.
10. Ujj, L., Devanathan, S., Meyer, T. E., Cusanovich, M. A., Tollin, G., and Atkinson, G. H. (1998) New photocycle intermediate in the photoactive yellow protein from *Ectorhodospira halophila:* Picosecond transient absorption spectroscopy, *Biophys. J. 75*, 406−412.
11. Hendriks, J., van Stokkum, I. H. M., and Hellingwerf, K. J. (2003) Deuterium isotope effects in the photocycle transitions of the photoactive yellow protein, *Biophys. J. 84*, 1180−1191.
12. Otto, H., Hoersch, D., Meyer, T. E., Cusanovich, M. A., and Heyn, M. P. (2005) Time-resolved single tryptophan fluorescence in photoactive yellow protein monitors changes in the chromophore structure during the photocycle via energy transfer, *Biochemistry 44*, 16804−16816.
13. Xie, A., Kelemen, L., Hendriks, J., White, B. J., Hellingwerf, K. J., and Hoff, W. D. (2001) Formation of a new buried charge drives a large-amplitude protein quake in photoreceptor activation, *Biochemistry 40*, 1510−1517.
14. Borucki, B., Devanathan, S., Otto, H., Cusanovich, M. A., Tollin, G., and Heyn, M. P. (2002) Kinetics of proton uptake and dye binding by photoactive yellow protein in wild type and in the E46Q and E46A mutants, *Biochemistry 41*, 10026−10037.
15. Rubinstenn, G., Vuister, G. W., Mulder, F. A. A., Dux, P. E., Boelens, R., Hellingwerf, K. J., and Kaptein, R. (1998) Structural and dynamic changes of photoactive yellow protein during its photocycle in solution, *Nat. Struct. Biol. 5*, 568−570.
16. Lee, B.-C., Croonquist, P. A., Sosnick, T. R., and Hoff, W. D. (2001) PAS domain receptor photoactive yellow protein is converted to a molten globule state upon activation, *J. Biol. Chem. 276*, 20821−20823.
17. Imamoto, Y., Kamikubo, H., Harigai, M., Shimizu, N., and Kataoka, M. (2002) Light-induced global conformational change of photoactive yellow protein in solution, *Biochemistry 41*, 13595−13601.
18. Brudler, R., Rammelsberg, R., Woo, T. T., Getzoff, E. D., and Gerwert, K. (2001) Structure of the I_1 early intermediate of photoactive yellow protein by FTIR spectroscopy, *Nat. Struct. Biol. 8*, 265−270.
19. Meyer, T. E., Tollin, G., Hazzard, J. H., and Cusanovich, M. A. (1989) Photoactive yellow protein from the purple phototrophic bacterium, *Ectothiorhodospira halophila*: Quantum yield of photobleaching and effects of temperature, alcohols, glycerol, and sucrose on kinetics of photobleaching and recovery, *Biophys. J. 56*, 559−564.
20. Meyer, T. E., Yakali, E., Cusanovich, M. A., and Tollin, G. (1987) Properties of a water-soluble, yellow protein isolated from a halophilic phototrophic bacterium that has photochemical activity analogous to sensory rhodopsin, *Biochemistry 26*, 418−423.
21. Unno, M., Kumauchi, M., Sasaki, J., Tokunaga, F., and Yamauchi, S. (2000) Evidence for a protonated and cis configuration chromophore in the photobleached intermediate of photoactive yellow protein, *J. Am. Chem. Soc. 122*, 4233−4234.
22. Pan, D., Philip, A., Hoff, W. D., and Mathies, R. A. (2004) Time-resolved resonance Raman structural studies of the pB′ intermediate in the photocycle of photoactive yellow protein, *Biophys. J. 86*, 2374−23283.
23. Genick, U. K., Devanathan, S., Meyer, T. E., Canestrelli, I. L., Williams, E., Cusanovich, M. A., Tollin, G., and Getzoff, E. D. (1997) Active site mutants implicate key residues for control of color and light cycle kinetics of photoactive yellow protein, *Biochemistry 36*, 8−14.
24. Borucki, B., Otto, H., Joshi, C. P., Gasperi, C., Cusanovich, M. A., Devanathan, S., Tollin, G., and Heyn, M. P. (2003) pH dependence of the photocycle kinetics of the E46Q mutant of photoactive yellow protein: Protonation equilibrium between the I_1 and I_2 intermediates, chromophore deprotonation by hydroxyl uptake, and protonation relaxation in the dark state, *Biochemistry 42*, 8780−8790.
25. Borucki, B., Kyndt, J. A., Joshi, C. P., Otto, H., Meyer, T. E., Cusanovich, M. A., and Heyn, M. P. (2005) Effect of salt and pH on the activation of photoactive yellow protein and gateway mutants Y98Q and Y98F, *Biochemistry 44*, 13650−13663.
26. Harigai, M., Imamoto, Y., Kamikubo, H., Yamazaki, Y., and Kataoka, M. (2003) Role of an N-terminal loop in the secondary structural change of photoactive yellow protein, *Biochemistry 42*, 13893−13900.
27. Imamoto, Y., Harigai, M., and Kataoka, M. (2004) Direct observation of the pH-dependent equilibrium between L-like and M intermediates of photoactive yellow protein, *FEBS Lett. 577*, 75−80.
28. Miller, A., Leigeber, H., Hoff, W. D., and Hellingwerf, K. J. (1993) A light-dependent branching reaction in the photocycle of the yellow protein from *Ectothiorhodospira halophila*, *Biochim. Biophys. Acta 1141*, 190−196.
29. Hendriks, J., Hoff, W. D., Crielaard, W., and Hellingwerf, K. J. (1999) Protonation deprotonation reactions triggered by photoactivation of photoactive yellow protein from *Ectothiorhodospira halophila*, *J. Biol. Chem. 274*, 17655−17660.
30. Joshi, C. P., Borucki, B., Otto, H., Meyer, T. E., Cusanovich, M. A., and Heyn, M. P. (2005) Photoreversal kinetics of the I_1 and I_2 intermediates in the photocycle of photoactive yellow protein by double flash experiments with variable time delay, *Biochemistry 44*, 656−665.
31. Borucki, B., Otto, H., and Heyn, M. P. (1999) Reorientation of the retinylidene chromophore in the K, L, and M intermediates of bacteriorhodopsin from time-resolved linear dichroism: Resolving kinetically and spectrally overlapping intermediates of chromoproteins, *J. Phys. Chem. B 103*, 6371−6383.
32. Kyndt, J. A., Vanrobaeys, F., Fitch, J. C., Devreese, B. V., Meyer, T. E., Cusanovich, M. A., and Van Beeumen, J. J. (2003) Heterologous production of *Halorhodospira halophila* holophotoactive yellow protein through tandem expression of the postulated biosynthetic genes, *Biochemistry 42*, 965−970.
33. Dickopf, S., and Heyn, M. P. (1997) Evidence for the first phase of the reprotonation switch of bacteriorhodopsin from time-resolved photovoltage and flash photolysis experiments on the photoreversal of the M-intermediate, *Biophys. J. 73*, 3171−3181.
34. Hendler, R. W., and Shrager, R. I. (1994) Deconvolutions based on singular value decomposition and pseudo inverse: A guide for beginners, *J. Biochem. Biophys. Methods 78*, 1−33.
35. Henry, E. R., and Hofrichter, J. (1992) Singular value decomposition: Application to analysis of experimental data, *Methods Enzymol. 210*, 129−192.
36. Borucki, B., Otto, H., Rottwinkel, G., Hughes, J., Heyn, M. P., and Lamparter, T. (2003) Mechanism of Cph1 phytochrome assembly from stopped-flow kinetics and circular dichroism, *Biochemistry 42*, 13684−13697.
37. Meyer, T. E., Devanathan, S., Woo, T., Getzoff, E. D., Tollin, G., and Cusanovich, M. A. (2003) Site-specific mutations provide new insights into the origin of pH effects and alternative spectral forms in the photoactive yellow protein from *Halorhodospira halophila*, *Biochemistry 42*, 3319−3325.
38. Demchuk, E., Genick, U. K., Woo, T. T., Getzoff, E. D., and Bashford, D. (2000) Protonation states and pH titration in the photocycle of photoactive yellow protein, *Biochemistry 39*, 1100−1113.
39. Druckmann, S., Heyn, M. P., Lanyi, J. K., Ottolenghi, M., and Zimanyi, L. (1993) Thermal equilibrium between the M and N intermediates in the photocycle of bacteriorhodopsin, *Biophys. J. 65*, 1231−1234.
40. Unno, M., Kumauchi, M., Hamada, N., Tokunaga, F., and Yamauchi, S. (2004) Resonance Raman evidence for two conformations involved in the L intermediate of photoactive yellow protein, *J. Biol. Chem. 279*, 23855−23858.

BI0517335